

University of Dundee

Roughness threshold for cell attachment and proliferation on plasma micro-nanotextured polymeric surfaces

Bourkoula, A.; Constantoudis, V.; Kontziampasis, D.; Petrou, P. S.; Kakabakos, S. E.; Tserepi, A.

Published in:
Journal of Physics D: Applied Physics

DOI:
[10.1088/0022-3727/49/30/304002](https://doi.org/10.1088/0022-3727/49/30/304002)

Publication date:
2016

Document Version
Peer reviewed version

[Link to publication in Discovery Research Portal](#)

Citation for published version (APA):

Bourkoula, A., Constantoudis, V., Kontziampasis, D., Petrou, P. S., Kakabakos, S. E., Tserepi, A., & Gogolides, E. (2016). Roughness threshold for cell attachment and proliferation on plasma micro-nanotextured polymeric surfaces: The case of primary human skin fibroblasts and mouse immortalized 3T3 fibroblasts. *Journal of Physics D: Applied Physics*, 49(30), Article 304002. <https://doi.org/10.1088/0022-3727/49/30/304002>

General rights

Copyright and moral rights for the publications made accessible in Discovery Research Portal are retained by the authors and/or other copyright owners and it is a condition of accessing publications that users recognise and abide by the legal requirements associated with these rights.

Take down policy

If you believe that this document breaches copyright please contact us providing details, and we will remove access to the work immediately and investigate your claim.

1 **Roughness threshold for cell attachment and proliferation**
2 **on plasma micro-nanotextured polymeric surfaces: the case**
3 **of primary human skin fibroblasts and mouse immortalized**
4 **3T3 fibroblasts**

5
6 A. Bourkoula^{1*}, V. Constantoudis^{2*}, D. Kontziampasis^{2**}, P.S. Petrou¹,
7 S.E. Kakabakos¹, A. Tserepi², E. Gogolides²

8 ¹Immunoassay/Immunosensors Lab, Institute of Nuclear and Radiological Sciences
9 and Technology, Energy and Safety, NCSR “Demokritos”, 153 41 Aghia Paraskevi,
10 Attiki, Greece

11 ²Institute of Nanoscience & Nanotechnology, NCSR “Demokritos”, 153 41 Aghia
12 Paraskevi, Attiki, Greece

13
14 *These authors contributed equally in this study.

15 ⁺Author current address: Institute of Particle Science and Engineering (IPSE)
16 School of Chemical and Process Engineering (SCAPE)
17 Room 2.15, Engineering Building,
18 University of Leeds,
19 Leeds, LS2 9JT, UK

20
21
22 Corresponding author: Dr Evangelos Gogolides

23 Institute of Nanoscience and Nanotechnology
24 NCSR “Demokritos”
25 Patriarhou Gregoriou & Neapoleos 27 Street
26 Aghia Paraskevi, Attiki, Greece 153 41
27 Tel: +30-210-6503237, fax: +30-210-6511723
28 E-mail: e.gogolides@inn.demokritos.gr

30 **Abstract**

31 Poly(methyl methacrylate) surfaces have been micro-nanotextured in oxygen plasmas with
32 increasing ion energy, leading to micro-nanotopography characterized by increased root mean
33 square roughness, correlation length and fractal dimension. Primary Human skin fibroblasts
34 and mouse immortalized 3T3 fibroblasts were cultured on these surfaces and the number of
35 adhering cells, their proliferation rate and morphology (cytoplasm and nucleus area) were
36 evaluated as a function of roughness height, correlation length, and fractal dimension. A
37 roughness threshold behavior was observed for both types of cells leading to dramatic cell
38 number decrease above a threshold, which is almost similar for the two types of cells, despite
39 their differences in size and stiffness. Results are discussed based on two theoretical models,
40 which are reconciled and unified when the elastic moduli and the size of the cells are taken
41 into account.

42

43

44

45

46

47

48

49

50

51

52

53

54 **1. Introduction**

55 In vivo, cells are never exposed to flat surfaces, but reside in an environment composed of
56 wide ranges of nanoscale surface roughness and submicrometer sized fibrils, since the
57 basement membranes of tissues exhibit nanotopographies which interact with cells [1]. It is
58 therefore very important to be able to create nanostructured surfaces that are more biomimetic
59 compared to standard flat culture surfaces [2]. The recent developments of micro- and nano-
60 fabrication technologies offer many possibilities for the application of nanostructured surfaces
61 in the fields of tissue engineering [3, 4], medical prosthetics [5], biochips for diagnostics [6,
62 7], and cell microarrays [8].

63 Many techniques have been developed for the fabrication of substrates with controlled
64 nanoscale topography and surface chemistry [9], such as electron beam lithography [10],
65 colloidal lithography [11], dip-pen lithography [12], micro-contact printing [13], polymer
66 demixing [14], photolithography [5] and electrospinning [15]. However, the requirement for
67 rapid and reproducible fabrication of nano-features at low cost is met only by a few methods.
68 Plasma treatment is such a method, due to the number of parameters that can be altered to
69 achieve the desired morphological and chemical effects. Changing feed gas in the plasma, and
70 bias voltage (which determines the energy of the positive ions inducing ion-enhanced etching
71 of the substrate) one may have different modification ranging from deposition to etching,
72 nanotexturing, chemical modification, and consequently wetting control [16-20]. Plasma
73 etching and plasma nanoassembly enables fast (within a few minutes) fabrication of random
74 or quasi-ordered nanostructures on polymeric surfaces [21-23].

75 There are numerous experimental studies on the effect of surface topography (both random
76 and ordered) on cell behavior leading to a variety of conclusions mainly due to the high
77 number of parameters that could affect cell behavior (cell type, feature size and geometry,
78 properties of the bulk material, etc.) [1, 5]. In particular, some works report an increase of cell
79 adhesion and proliferation with roughness [24], while others indicate the existence of an
80 optimum range of roughness to efficiently capture cells and enhance their adhesion and
81 proliferation [25, 26]. On the other hand, there are reports that show the opposite behavior
82 with reduced cell growth on largely rough substrates [27-32]. Besides the impact of
83 roughness, induced mechanical stimuli on cell adhesion and proliferation, it is important to
84 know the effects on the inner cell structure since these changes may control the adhesion
85 process. However, while there are several reports discussing cell adhesion and proliferation
86 on rough surfaces, there are only a few reports discussing the effects of roughness on the
87 morphology of the cytoplasm and the nucleus [33, 34].

88 The above mentioned variety of results and conclusions makes it difficult to summarize the
89 effect of nanotopography on cell behavior in a concise and complete framework. Despite this
90 difficulty, in a recent study Decuzzi and Ferreira [35] elaborated a theoretical model to
91 improve our understanding on cell – topography interaction and offer a unified explanation of
92 the above diverse results. Their approach is mainly based on the estimation of the free energy
93 balances between cell membrane and substrate surface, assuming that cells are thin elastic
94 layers with specific Young modulus (E), which reside on a solid rough surface with periodic
95 morphology. In particular, a critical roughness threshold exists above which cells cannot
96 survive on the topography. The threshold is shown to be inversely proportional to E , which
97 means that given similar adhesion forces, less rigid cells (with smaller E) adhere more on the
98 substrate protrusions and have a higher threshold.

99 A different model has been motivated by the bactericidal property of the nanopatterned
100 Cicada wing surfaces and developed by E.P. Ivanova and her group [36, 37]. They proposed
101 that the adsorption of the bacterial cells on the nanopattern of cicada wing may lead to a
102 drastic enhancement of their area causing the stretching of cell membrane. When the
103 stretching exceeds some threshold, it can cause the irreversible rupture of cell surface and its
104 death. According to this modeling approach, the less rigid (i.e. with small E) bacterial
105 membranes are more sensitive to the bactericidal mechanism of the wings and present
106 increased death rates.

107 The impact of cell membrane stiffness on cell adhesion differentiates the two models since
108 they predict opposite trends. A combination of the effects of both models (increased adhesion
109 and stretching) can lead to milder dependencies of critical roughness threshold on cell
110 stiffness. An experimental verification of the synergetic role of both effects would require to
111 culture cells with different stiffness and similar adhesion forces on the same series of surfaces
112 with increased roughness. This is what this work is aiming towards.

113 In particular, the goal of this work is to evaluate the effect of surface roughness on the
114 attachment and proliferation of two different types of fibroblasts, namely human primary skin
115 fibroblasts and mouse 3T3 immortalized fibroblasts, and discuss the results with respect to the
116 free-energy based theoretical scheme. The selection of the specific cells was based on the fact
117 that although they are both fibroblasts and could be cultured under common conditions they
118 differ considerably in size and stiffness, with the human skin fibroblasts to be considerably
119 bigger and more elastic than the mouse immortalized fibroblasts [38]. In addition to cell
120 adhesion and proliferation, here the surface roughness effects on the morphology of both the
121 cytoplasm and the nucleus of cells are also determined, so as to inspect in more details the

122 very nature of cell response caused by roughness undulations. The rough substrates we
123 employed in this study were poly(methyl methacrylate) (PMMA) films treated and micro-
124 and nano-textured by oxygen plasma with a root mean square surface roughness R_{rms} from ~5
125 to 40 nm depending on the treatment time. A threshold behavior is demonstrated regarding
126 cell adhesion, proliferation as well as cell morphological characteristics versus topography,
127 and these findings are reconciled with the theoretical calculations mentioned above.
128 Although PMMA is not a commonly used biomaterial for cell cultures, it is extensively used
129 for microfluidics and lab-on-a-chip fabrication. It is therefore very important for those
130 working with cells on chip to know the PMMA cell binding properties, given the great
131 interest for incorporation of such “smart” surfaces into microfluidics [20].

132

133 **2. Methods**

134 **2.1 PMMA surface preparation**

135 Poly(methyl methacrylate) (PMMA) with molecular weight of 120 kDa (Sigma-Aldrich Co;
136 Taufkirchen, Germany) was dissolved at 30% (w/w) in anhydrous Propylene Glycol Methyl
137 Ether Acetate (PGMEA) and spin-coated on Si wafers (1000 rpm for 30 s with acceleration of
138 300 rpm/s²), resulting in a film thickness of ~20 μm . After spin-coating the wafers were baked
139 at 90 °C for 20 min and then at 150 °C for 1h. Etching was performed in a high density
140 helicon plasma reactor (MET system from Alcatel-Adixen) at the following conditions:
141 Oxygen gas flow rate 100 sccm; operating pressure 0.75 Pa; electrode temperature 60 °C; bias
142 voltage varying from -25 to -100 V (to find the value of ion energy the plasma potential of
143 15-25 V should be added to the absolute value of the bias voltage, e.g., 25V+15V, or
144 100V+15V). The etching time was in all cases 1 min and the etching rate varied between 500-
145 1500 nm/min depending on the bias voltage. Temperature was controlled by helium backside
146 cooling of a carrier wafer on which samples were glued with thermal paste.

147

148 **2.2 Surface characterization**

149

150 PMMA surfaces were analyzed by a CP-II AFM instrument from Veeco (Plainview, NY). All
151 AFM measurements were performed in (non-contact) tapping mode using PPP-NCHR-50 tips
152 with radius of curvature less than 10 nm. The obtained surface measurements have the form
153 of measured heights on a x-y square lattice $z(x_i, y_j)$ where $i, j=1, \dots, N$. In our measurements N
154 = 512 while the scanning range (lattice area) has been $2 \times 2 \mu\text{m}^2$. Due to the random and
155 complex nature of surface morphologies statistical analysis, as well as mathematical

156 transformations are needed for their characterization. To this end, the software nanoTOPO-
157 AFM was used (Nanometrisis; Athens, Greece, www.nanometrisis.com), which delivers
158 several roughness metrics characterizing both vertical (amplitude) and spatial (frequency)
159 aspects of surface morphology. In this work, the focus was on three parameters, root mean
160 square (rms), correlation length and fractal dimension, which define the most dominant
161 features of surfaces. Rms value quantifies the amplitude of height fluctuations on surfaces and
162 with the mean amplitude R_a they constitute the most common roughness parameters. In a
163 more mathematical perspective, rms is the second order moment of the surface height
164 distribution function. The second parameter is the correlation length ξ which defines the
165 lateral distance beyond which the in-plane surface height correlations degrade to noise levels.
166 In surfaces with random distribution of well-defined mounds, the correlation length can be
167 used as an estimator of the average mound width. The fractal dimension d_f can be calculated
168 in fractal surfaces exhibiting self-similar (more precisely self-affine) symmetry and quantifies
169 the relative contribution of high frequency fluctuations to the total surface roughness. The
170 triplet of these parameters (rms, ξ , d_f) constitute the so-called three-parameter model which
171 has been extensively used in the characterization of sidewall roughness in nanoelectronic
172 structures [39].

173 In order to probe the chemical modification of the surface by the plasma, Fourier Transform
174 Infrared Spectroscopy (FTIR) was performed with a Thermo Scientific Nicolet 6700 FT-IR
175 instrument using attenuated total reflection (ATR) technique (128 scans, resolution of 4.0 cm^{-1}
176 $^{-1}$, data recorded from 4000 cm^{-1} to 450 cm^{-1}).

177

178 **2.3 Cell culture**

179

180 Primary human skin fibroblasts and Swiss albino mouse immortalized 3T3 fibroblasts were
181 obtained by the American Type Culture Collection. Cells were grown in Dulbecco modified
182 Eagle medium (DMEM) supplemented with 10% (v/v) heat-inactivated fetal bovine serum
183 (FBS), 2 mM L-glutamine, and 1% (v/v) penicillin/streptomycin solution at 37 °C in a
184 saturated humid atmosphere containing 95% air and 5% CO_2 . When cells reached 70-80 %
185 confluence, they were detached from the culture flasks through treatment with 0.25 % (w/v)
186 trypsin/EDTA solution and re-suspended in DMEM.

187

188 **2.4 Cell adhesion experiments**

189

190 Untreated and plasma nanotextured PMMA surfaces were used as substrates to culture mouse
191 immortalized 3T3 fibroblasts and primary human skin fibroblasts. The plasma treated PMMA

192 surfaces were left to age for at least 10 days prior to use so as to reach a constant contact
193 angle very close to that of untreated PMMA (~67°). The wafers with the PMMA films were
194 cut to 1x1 cm² pieces. These pieces were sterilized prior to cell seeding by exposure to
195 ultraviolet light for 20 min and placed in 24-well culture plates. For seeding 1 mL of cells
196 suspension at a density of 25,000 cells/mL was added in each well. The culture medium in the
197 wells was renewed every 24 h. To determine the number of attached cells, the substrates were
198 washed with 10 mM phosphate buffer saline, pH 7.4 (PBS), in order to remove the non-
199 adhered dead cells. Then, the cells were fixed with 4% (w/v) paraformaldehyde solution in
200 PBS for 20 min at room temperature (RT). The fixed cells were rinsed 3 times with PBS and
201 incubated with a 50 ng/ml of 4',6-diamidino-2-phenylindole (DAPI; Sigma-Aldrich Co.,
202 Taufkirchen, Germany) in PBS for 10 min at RT to stain the cell nucleus. Thereafter,
203 coverslips were mounted on top of the substrates using p-Phenylenediamine antifade
204 mounting gel (Vectashield; Vector Laboratories Inc., Burlingame, CA). The substrates were
205 observed using an epifluorescence microscope (Axioskop 2 Plus; Carl Zeiss, Hamburg,
206 Germany) facilitated with a filter pair with appropriate excitation/emission maximums for
207 DAPI (365/420 nm) and a CCD camera (MicroPublisher 3.3 RTV; QImaging, Surrey, BC,
208 Canada) for image acquisition. For each surface 25 images were obtained, each one covering
209 a 1725x1291 μm² area. From these images the stained cell nuclei were counted using Image
210 ProPlus v6.0 software (Media Cybernetics, Inc.; Rockville, MD). Experiments were
211 performed three times in quadruplicate and the numbers of cells counted were averaged and
212 expressed as cells/cm² (mean ± standard deviation). The results were analyzed statistically by
213 paired Student's t-test method and considered significantly different at p values lower than
214 0.05.

215

216 **2.5 Cell morphological analysis**

217 Fluorescence staining was employed to image the cytoskeleton and the nucleus of the primary
218 human skin and mouse immortalized 3T3 fibroblasts adhered on the different PMMA
219 surfaces after 3 days of culture. For this purpose after washing and fixing of cells with
220 paraformaldehyde as described in 2.4, the cells were rinsed 3 times with PBS and
221 permeabilized through incubation with 0.1% (v/v) Triton X-100 in PBS for 10 min. After
222 gentle washing with PBS, the cells were blocked with 5% (v/v) bovine serum albumin
223 solution in PBS for 1h at RT, and then washed with PBS. To visualize the cytoskeleton, F-
224 actin was stained through reaction with a 150 nM Phalloidin Atto 488 (Sigma-Aldrich Co.;
225 Taufkirchen, Germany) solution in PBS for 1 h, followed by washing with PBS. Staining of
226 the nucleus with DAPI and mounting of the coverslips was performed as described in 2.4.

227 Fluorescence images were obtained using two filter pairs with appropriate excitation/emission
228 maximums (365/420 nm for DAPI, 493/520 nm for Atto 488). Images covering a 430 x 325
229 μm^2 area were obtained, and the cytoplasm and nucleus area of at least 200 random individual
230 cells per substrate were calculated using the Image ProPlus v6.0 software. Experiments were
231 performed three times in quadruplicate, and the cells cytoplasm and nucleus area determined
232 were averaged and expressed as mean value \pm standard deviation.

233

234

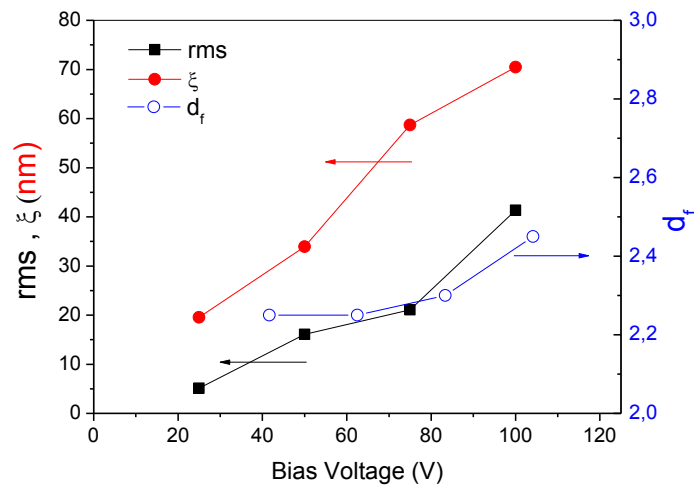
235 **3. Results**

236 **3.1 Oxygen plasma micro-nanotextured surfaces with increasing roughness**

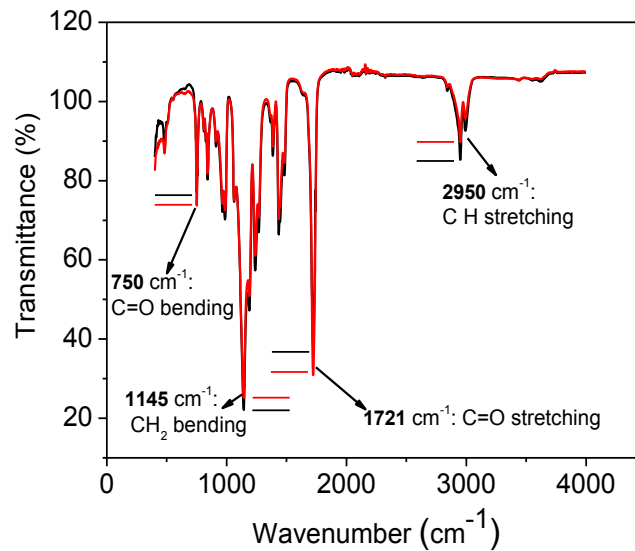
237 PMMA substrates were etched in oxygen plasma for 1 min using four different bias voltages
238 (-25, -50, -75 and -100 Volts) while keeping all other parameters fixed. The plasma treatment
239 causes gradual roughening of the etched PMMA surfaces, while roughness parameters (rms,
240 ξ , d_f) grow with bias voltage as shown in Figure 1a. All roughness parameters exhibit a
241 correlated behavior with an almost linear growth versus bias voltage. This means that at high
242 bias voltages the roughness (texture) becomes higher, with wider features, and with higher
243 frequency undulations on these features. Detailed AFM imaging was presented in one of our
244 previous publications [34].

245 The plasma modifies both the surface topography and the surface chemistry. Detailed XPS
246 analysis of oxygen plasma treated PMMA has been discussed in detail in our previous work
247 [17, 41]. Here, in Fig. 1b we also present FTIR data to show the plasma modification. The
248 FTIR spectra of PMMA confirmed the presence of various bonds in the structure (see Figure
249 1b). PMMA give a series of characteristic infrared bands at 2950, 1722, 1435, 1386, 1238,
250 1190, 1142, 986, 840, 810 and 751 cm^{-1} [42,43]. Although the two spectra revealed similar
251 peaks, there are differences in the peak height as shown in the Fig. 1b. The bands at 2950 and
252 1145 cm^{-1} assigned to CH stretching, and CH_2 bending, respectively, are reduced in size
253 (transmittance increases) due to etching of the material and oxidation of the surface. On the
254 contrary the intense band at 1721 cm^{-1} assigned to C=O stretching (skeletal mode), and the
255 medium size band at 750 cm^{-1} assigned to the C=O in plane and out of plane bending,
256 increase in size (transmittance decreases) due to the strong surface oxidation to CO and
257 COOH groups.

a



b



258 **Figure 1.** a) Surface roughness parameters of PMMA surfaces micro-nanotextured in Oxygen
 259 plasma (rms, correlation length ξ , and fractal dimension d_f) versus bias voltage. Notice the
 260 correlated behaviour of all roughness parameters which show an almost linear increase with
 261 bias voltage. b) ATFTIR spectra of untreated (black line) and plasma treated PMMA films
 262 (red line). Notice the reduction of the CH and CH₂ peaks and the increase of the C=O peaks
 263 after plasma treatment.

264

265

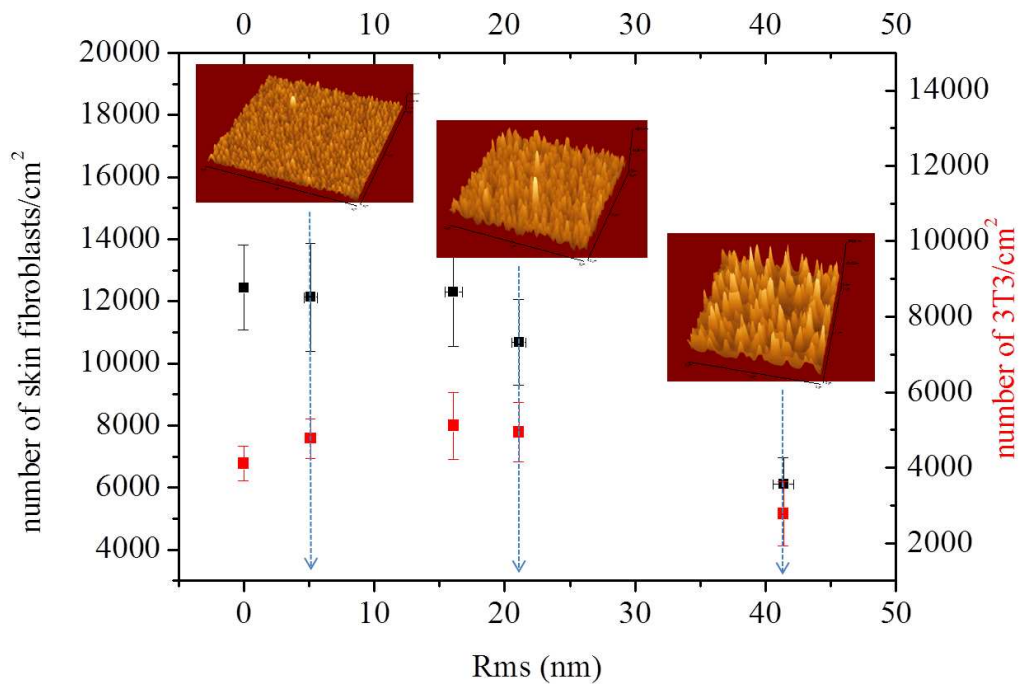
266

267 **3.2 Adhesion and proliferation of primary human skin and mouse immortalized 3T3**
268 **fibroblasts on oxygen plasma micro-nanotextured PMMA surfaces**

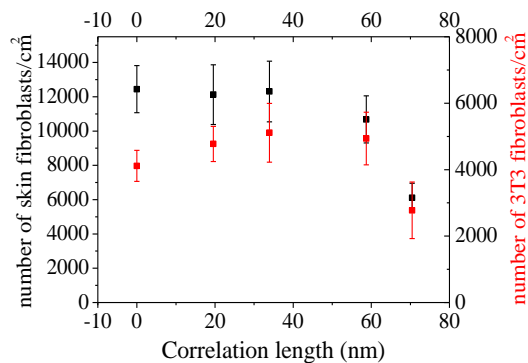
269 The micro-nanotextured PMMA surfaces along with the untreated ones were used as culture
270 substrates for primary human skin fibroblasts or mouse immortalized 3T3 fibroblasts. After
271 one and three days of culture under standard conditions, the number of cells on the different
272 surfaces was determined. Concerning skin fibroblasts after 1 day of culture, it was found that
273 similar numbers of cells were adhered on all plasma treated and untreated surfaces (5890 ± 524
274 cells per cm^2). After 3 days of culture, as shown in Figure 2(a-c), the number of skin
275 fibroblasts on the untreated as well as on substrates with rms, ξ and d_f values lower than or
276 equal to 21.1 nm, 40 nm and 2.25, respectively, was increased by a factor of approximately 2.
277 On the contrary, when they were cultured on the more roughened substrates (rms=41.4 nm,
278 $\xi=70.4$ nm and $d_f=2.45$ nm) a significant reduction of the number of attached cells was
279 observed compared to surfaces with lower roughness. In detail, the number of attached cells
280 per unit area was almost half in the strongly rough substrates with respect to the surfaces with
281 lower or no roughness at all (untreated PMMA films).

282 The picture changes slightly when we move to 3T3 cells. After 1 day of culture, the number
283 of cells adhered on plasma treated surfaces were similar and at least 4-times higher
284 (6938 ± 789) than the number on the untreated PMMA surface (1664 ± 312). Nevertheless,
285 looking at the cell densities after three days of culture (red squares in Figure 2), we noticed
286 that similarly to fibroblasts, the strongly rough substrates (rms=41.4 nm, $\xi=70.4$ nm and
287 $d_f=2.45$ nm) are hostile for 3T3 and the density drops to almost 60% of the surfaces with
288 smaller roughness. In contrast, the number of cells on the untreated PMMA after 3-days of
289 culture is almost 2-times higher than that determined for 1-day of culture. Thus, in order to
290 deduce differences in cell behavior due to plasma treatment, the proliferation rate was
291 determined as the ratio of the number of cells counted on a particular surface after 3 days of
292 culture to the number determined after 1 day of culture.

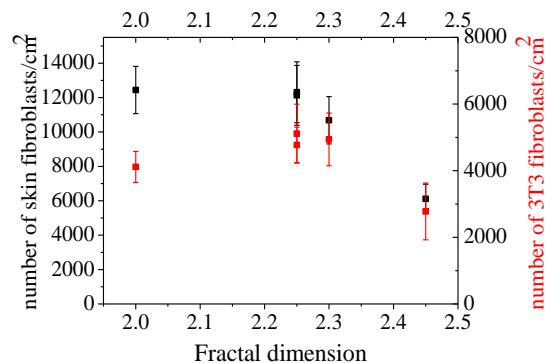
A



B



C

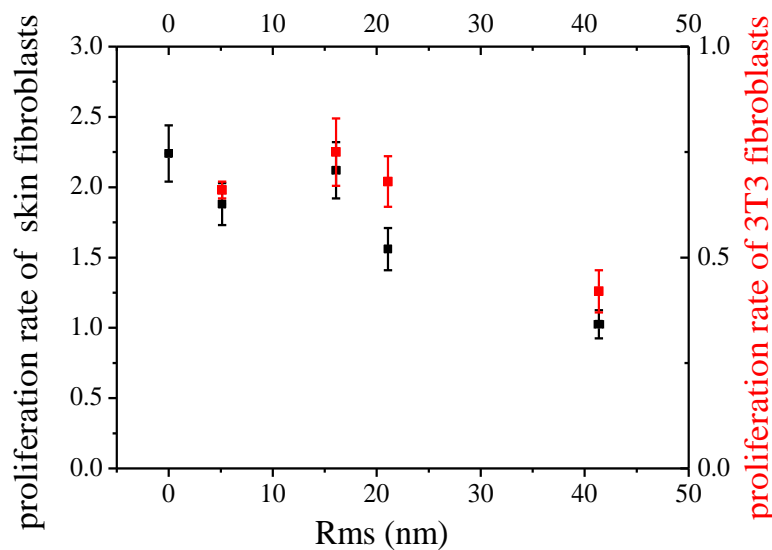


293 **Figure 2.** The number of primary skin fibroblasts (black full squares) and 3T3 cells (red full
 294 squares) per surface unit as a function of surface rms (a), fractal dimension (b), and
 295 correlation length (c) after 3 days of culture. AFM images of surface topography are shown in
 296 Figure 2(a) for 3 substrates with 3 different rms values (left 5.14 nm; center 21.1 nm; and
 297 right 41.4 nm). Each point is the mean value of three independent experiments performed in
 298 quadruplicate \pm SD.

299

300 The proliferation rate versus the rms value of the different PMMA substrates (shown in
 301 Figure 3) demonstrate that for the primary skin fibroblasts the rate was decreased
 302 approximately by 50% when cells were cultured on the PMMA surface with the highest
 303 nanostructure (rms=41.4 nm) compared to all the other nanotextured (rms=5.14-21.1 nm) as

304 well as the untreated PMMA surfaces which exhibited proliferation rates of about 2 (see black
 305 squares in Figure 3). On the other hand, the proliferation rates determined for 3T3
 306 demonstrate that even a slight roughening of PMMA substrates (rms=5.14 nm) influences
 307 negatively the proliferation of cells since the rate was three-fold lower on the surface with the
 308 lowest roughness (proliferation rate=0.7) compared to the one determined for the untreated
 309 PMMA surface (proliferation rate=1.9, not shown in Figure 3). Similar proliferation rates
 310 were obtained for surfaces with rms, ξ and d_f values lower than or equal to 21.1 nm, 40 nm
 311 and 2.25, respectively, whereas for the surface with the higher roughness (rms=41.4 nm,
 312 ξ =70.4 nm and d_f =2.45 nm), the rate was dropped to less than 0.5. Rate values smaller than 1
 313 suggest that the roughening of PMMA substrates promotes cell death, and therefore leads to a
 314 net reduction of their population. Thus, concerning the rough substrates, an rms value higher
 315 than 21.1 nm, seems to affect negatively the proliferation of both skin fibroblasts and 3T3
 316 cells. The fact that for 3T3 cells the proliferation rates for all plasma treated surfaces are
 317 lower than that on the untreated ones could be ascribed to a different response to surface
 318 chemistry of plasma treated PMMA. The above results for both cell adhesion and
 319 proliferation rate reveal the existence of a threshold in roughness parameters above which the
 320 surface roughness has detrimental effect on cell capture and proliferation.



321

322 **Figure 3.** Cell growth assessment of primary skin fibroblasts (black squares) and
 323 immortalized 3T3 fibroblasts (red squares) after culture on untreated PMMA (rms=0 nm) and
 324 on different nanotextured PMMA surfaces of increasing roughness. The proliferation rate of
 325 3T3 cells on untreated PMMA surface (1.9 ± 0.1) is not shown in the plot in order to visualize
 326 more clearly the cells behavior on the rough surfaces. Each point is the mean value of three
 327 independent experiments performed in quadruplicate \pm SD.

328 **3.3 Effect of PMMA surface roughness on primary human skin and mouse immortalized**
329 **3T3 fibroblasts morphology**

330 Further to cell attachment and proliferation, the effect of surface micro-nanotexturing on cell
331 and nucleus size was evaluated. For this purpose, double fluorescence staining of
332 cytoskeleton F-actin and cell nucleus was employed. Concerning skin fibroblasts, it was
333 found that the cell cytoplasm area (Figure 4(a)) and morphology remained unaffected when
334 the cells grew for 3 days on untreated PMMA, as well as on nanotextured PMMA surfaces
335 with rms values lower than or equal to 21.1 nm (Figure 4(b1) & 4(b2)). On the contrary, when
336 the cells were grown on the nanotextured PMMA surface with rms of 41.4 nm a significant
337 distortion of their cytoplasm was observed (Figure 4(b3)). It is worth noticing that on the
338 roughest PMMA surface, the cells cytoplasm area was reduced approximately 2.5 times
339 compared to the cytoplasm area determined for cells grown on either untreated or plasma
340 treated PMMA surfaces of lower roughness (Figure 4(a)). This is evident from the
341 representative cell images grown on nanotextured PMMA surfaces with rms values 5.14 nm,
342 21.1 nm and 41.4 nm, provided in Figures 4(b1), 4(b2), and 4(b3), respectively. From the
343 images it is also evident that when the cells have been grown on surfaces with rms values
344 lower than or equal to 21.1 nm, they were well spread on the surface and extend many
345 filopodia-type extensions. In addition, the F-actin filaments were well organized and oriented
346 along the cell long axis. On the other hand, the cells that have been cultured on the roughest
347 surface (rms value 41.4 nm) were significantly shrunk with no apparent F-actin organization
348 and only few and short filopodia-type extensions can be observed. Similarly to cell
349 cytoplasm, the nucleus was significantly shrunk (~40%) compared to other surfaces only
350 when the cells were cultured on the roughest surface (Figure 4(a)).

351

352

353

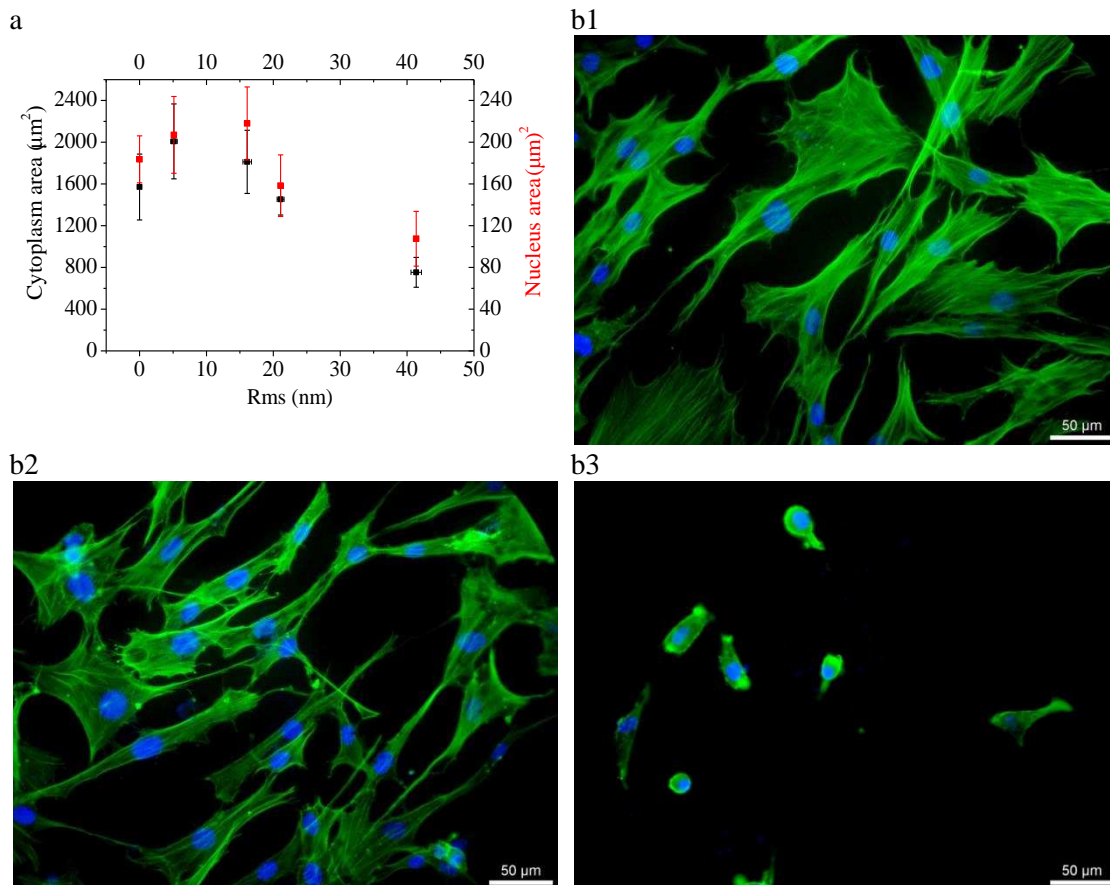
354

355

356

357

358



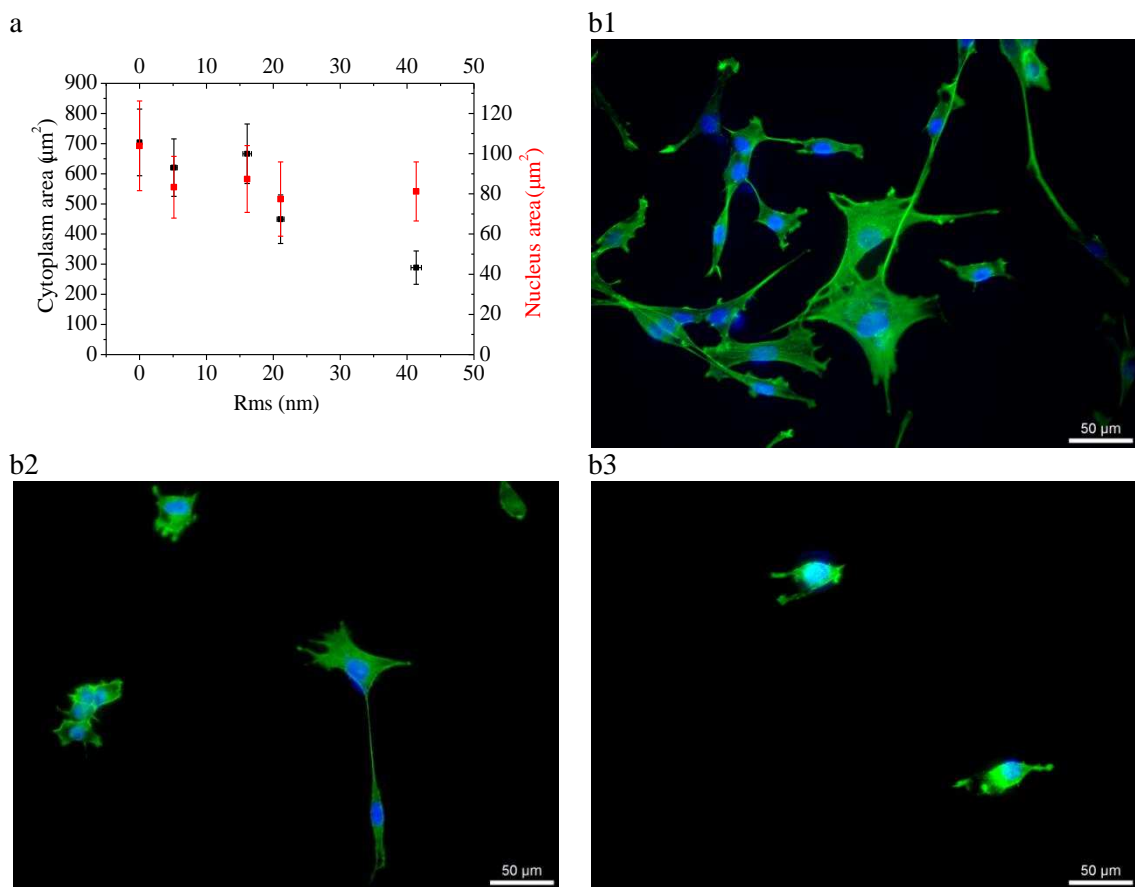
359

360 **Figure 4.** a) Cytoplasm and nucleus area of primary skin fibroblasts cultured for three days
 361 on PMMA surfaces versus surface roughness (Rms). Each point is the mean value of three
 362 independent experiments performed in quadruplicate \pm SD. b) Fluorescence microscope
 363 images of primary skin fibroblasts (nuclei: blue; cytoplasm: green) cultured for three days on
 364 oxygen-plasma nanotextured PMMA surfaces with rms 5.14 nm (b1), 21.1 nm (b2) and 41.4
 365 nm (b3).

366

367 Regarding 3T3 immortalized mouse fibroblasts, distinct differences in cell morphology were
 368 evident between cells cultured for 3 days on untreated and nanotextured surfaces with rms
 369 values ranging up to 16.1 nm compared to those cultured on surfaces with higher roughness
 370 (21.1 to 41.4 nm). As demonstrated in Figure 5(a), the cytoplasm area was reduced when cells
 371 were cultured on PMMA surfaces with rms values equal to or higher than 21.1 nm, compared
 372 to those cultured on surfaces with lower roughness or untreated PMMA surfaces. In particular
 373 as shown in Figure 5(a), the mean cytoplasm area of cells cultured on surfaces with rms value
 374 of 21.1 nm was reduced by 30% compared to that of cells cultured on untreated or PMMA
 375 surfaces with rms values of 5.14 and 16.1 nm, and by 60% when cells were cultured on the

376 roughest surface (rms 41.4 nm). Representative fluorescence images of 3T3 cells cultured for
 377 3 days on nanotextured PMMA surfaces with rms values of 5.14 nm, 21.1 nm and 41.4 nm,
 378 are provided in Figures 5(b1), 5(b2) and 5(b3), respectively. The cells presented normal
 379 morphology with well spread cytoskeleton on untreated PMMA surface as well as on
 380 substrates with rms values ranging between 5.14 and 16.1 nm. The cytoskeleton of 3T3 cells
 381 begun to shrink when they were cultured on PMMA surfaces with rms ≥ 21.1 nm (Figure
 382 5(b2)) and they presented the maximum shrinkage on the roughest PMMA (Figure 5(b3)).
 383 Nevertheless, opposite to the human skin fibroblasts, the shrinkage of the cell cytoplasm was
 384 not accompanied by shrinkage of the nucleus in the case mouse immortalized 3T3 fibroblasts.
 385



386

387 **Figure 5.** a) Cytoplasm and nucleus area of immortalized 3T3 fibroblasts cultured for three
 388 days on PMMA surfaces versus surface roughness (Rms). Each point is the mean value of
 389 three independent experiments performed in quadruplicate \pm SD. b) Fluorescence microscope
 390 images of immortalized 3T3 fibroblasts (nuclei: blue; cytoplasm: green) cultured for three
 391 days on oxygen-plasma nanotextured PMMA surfaces with Rms 5.14 nm (b1), 21.1 nm (b2)
 392 and 41.4 nm (b3).

393 4. Discussion

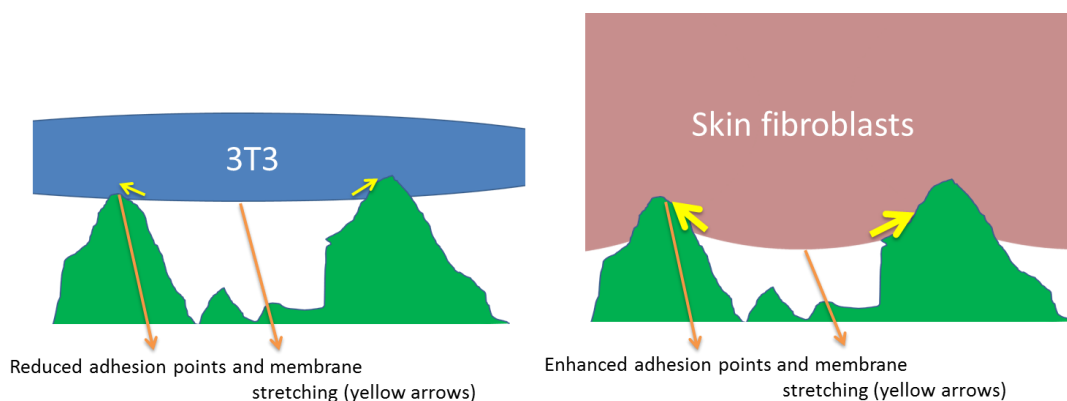
394

395 Recently several efforts have been undertaken towards an integrated framework for
396 understanding the impact of substrate morphology on cell adhesion. In the Introduction, we
397 made reference of two prominent theoretical approaches which elaborate a more biophysical
398 view of cell-surface interactions differentiating from the previous more biochemically-
399 oriented argumentations, since they consider them as interactions between an elastic bilayer
400 (cell membrane) and an inert solid rough substrate [35-37]. The basic theoretical prediction of
401 both models is the reduction of adhesion on substrates with large roughness (rms) above a
402 critical threshold value of rms_{cr} roughness. Below this threshold, we can have either
403 insensitivity of cell adhesion to roughness or a broad maximum indicating an optimum
404 surface roughness range for capturing cells. However, the two models and the mechanisms
405 they recall for explanation of experimental findings differ on the role of cell stiffness (Elastic
406 modulus E). According to the model proposed by Decuzzi and Ferrari [35], the rms_{cr} is
407 inversely proportional to adherent cell stiffness (E), which means that cells with less stiff
408 membranes require more substrate roughness to start reducing their adhesion strength. On the
409 other hand, the second model [36, 37] makes the opposite prediction and explains that the
410 bacteria cells with less stiff (smaller E) membranes suffer from more stretching and therefore
411 increased deterioration.

412 Looking again at the diagrams of Figure 2, one can realize that our experimental
413 measurements fit at least qualitatively with the basic theoretical predictions: both cell series
414 suffer from a reduction of their adhesion strength at the most rough substrates, with a critical
415 threshold roughly defined by $rms_{cr}=20$ nm, $\xi_{cr}=40-50$ nm and $d_{f,cr}=2.3$. Below the critical
416 threshold, the adhesion of 3T3 series exhibits a broad maximum, while skin fibroblasts
417 remain almost insensitive to substrate morphology changes. A threshold-like behaviour is also
418 observed in the dependencies of proliferation rate and cell cytoplasm and nucleus area on
419 substrate roughness (see Figs, 3, 4 and 5 respectively) since the PMMA surfaces with high
420 roughness deteriorate cell proliferation and reduce cytoplasm and nucleus spatial structure.
421 Therefore, the threshold in substrate roughness at $rms_{cr}=20$ nm, $\xi_{cr}=40-50$ nm and $d_{f,cr}=2.3$
422 impacts the whole aspects of cell life (adhesion, proliferation) and morphology (cytoplasm
423 and nucleus area). As referred above, this experimental finding agrees with the theoretical
424 predictions discussed in [35-37]. What needs more elucidation is the observed similarity of
425 threshold roughness values in the two cell series given their difference in membrane stiffness.

426 According to [38] the Young modulus of skin fibroblast cells is on average almost the half of
427 the modulus of 3T3 cells (~ 900 versus 1800 Pa). Given the expected similarity of the
428 strength of specific and nonspecific interactions in both cell types, the difference in cell
429 rigidities should have led to much larger roughness thresholds in skin fibroblasts. What is the
430 extra effect preventing it and causing the reduction of roughness threshold in this cell line?

431 At this point, we can recall the second modelling approach elaborating to explain the
432 bactericidal nature of cicada wing surface structures. As explained in the Introduction, the
433 adsorption of a bacteria cell on the surface structures of cicada wings could cause a drastic
434 stretching of the cell membrane especially on the suspended part between the contact points,
435 which could lead to irreversible cell membrane rupture and bacteria death. According to this
436 model, the less stiff the cell membrane is, the more detrimental is the effect of roughness and
437 the probability to rupture the cell membrane and cause its death. In addition to the stiffness
438 effect, a theoretical approach based on this model, has also shown that the detrimental
439 stretching of cell membrane is proportional to cell weight and size [40]. Taking into account
440 that the size of skin fibroblasts is almost twice the size of 3T3 cells, there is one more factor
441 causing the stretching effects to be much more severe in the fibroblasts than in the 3T3 cells.
442 A schematic of the membrane shape of both cell types when they are residing on a rough
443 substrate is illustrated in Figure 6. In this figure, it is shown that the smaller stiffness and the
444 larger size of skin fibroblasts favour larger adhesion areas on the summits of rough substrates
445 than the 3T3 cells. However, the same features (less stiffness and larger size) lead to stronger
446 stretching of cell membranes suspended between contact areas, which deteriorate cell
447 behaviour. These two effects can counteract each other providing an explanation of the
448 observed similarity of roughness thresholds in the number of captured cells (adhesion
449 strength) in the two series.



450

451 **Figure 6.** Schematic diagram of the membrane shapes of a 3T3 (left) and a fibroblast (right)
452 cell residing on a rough substrate. Due to the much larger stiffness and smaller size, 3T3 cell

453 is expected to develop less adhesion area with the substrate and to exhibit less stretching
454 between contact points than the skin fibroblasts (marked by the different width of yellow
455 arrows). The detrimental effect of increased stretching in skin fibroblasts can counteract the
456 enhanced adhesion areas and explain the similarity of roughness thresholds in two cell types.

457 The large stiffness of 3T3 cells can be also responsible for their reduced proliferation rates on
458 rough substrates with respect to those on flat surfaces (see 3.2). As shown in Figure 6, 3T3
459 cells are expected to exhibit a contact point configuration with the rough substrate due to their
460 large Young modulus which may lead to decreased adhesion strengths even for low values of
461 roughness.

462 A final comment concerns the role of substrate fractal dimension on cell adhesion. A recent
463 study has provided evidence that more fractality on substrate morphologies favors cell
464 adhesion [32]. On the contrary, here we observe that the strongly roughened substrates which
465 are characterized by increased fractal dimension are hostile to cell adhesion and give smaller
466 cell densities and proliferation rates. Following the authors of above ref. [32], we should
467 emphasize that the effect of fractal dimension is correlated to those of the height and width of
468 surface fluctuations as quantified by rms and ξ respectively. In our experiments, the surfaces
469 are modified by changing the bias voltages of plasma etching process and this lead to a
470 collective increase of all roughness parameters rms, ξ and d_f . Therefore, the large fractal
471 dimensions go with large rms and ξ values and we cannot see the bare effect of fractal
472 dimension at moderate roughness as suggested in [32]. The concluding message is that in
473 order to get a safe decision for the effects of a specific roughness parameter on cell adhesion,
474 we should be able to create surfaces on which we control the changes of this parameter in an
475 independent way. Otherwise, the effects of less important parameters (such as fractal
476 dimension) can be overwhelmed by the more dominant ones such as rms roughness.

477

478 **5. Conclusions**

479 Primary human skin fibroblasts and immortalized mouse 3T3 fibroblasts have been cultured
480 on oxygen plasma treated PMMA surfaces with random or quasi-ordered structures of
481 increasing roughness. The effect of surface roughness on the number of adhered cells, their
482 proliferation rate, as well as the morphology of cell cytoplasm and nucleus was determined.
483 Although the two cell types behaved differently on the rough surfaces, a common roughness
484 threshold was determined for surfaces with rms values higher than 20 nm above which the
485 cell adhesion, proliferation and morphology was significantly affected. Thus, in the case of

486 primary human fibroblasts, culture on the roughest surfaces led to the reduction of adhered
487 cell number and their proliferation rate, as well as to significant shrinkage of cell cytoplasm
488 and nucleus area, indicating a fatal effect of rough surfaces on these cells. On the other hand,
489 despite the fact that the number and proliferation of immortalized mouse 3T3 fibroblasts was
490 affected on all rough surfaces, the strongest effect was again observed when cells were
491 cultured on surfaces with rms values higher than 20 nm, where in addition a strong effect on
492 cell morphology was observed. Given the different stiffness and size of two cell types, the
493 similarity of roughness thresholds may seem puzzling. In an attempt to explain it, two
494 different theoretical approaches [35-37] have been reconciled emphasizing the double role
495 that elasticity and size may have in cell viability on rough surfaces: on one side, they enhance
496 adhesion areas on surface protrusions increasing the capturing strength while on the other
497 side, they induce more stretching of the suspended cell membrane deteriorating cell functions
498 and viability. These two effects can counteract and cause similar roughness thresholds in cell
499 series with different stiffness and size. The understanding of the response of different cell
500 types to nanotopography and the control of cell adhesion and morphology based on the effect
501 of substrate micro-nanotopography could provide essential information for the design of
502 novel materials [18, 20] for incorporation in “smart” microarrays, microfluidics, and lab on
503 chip devices for in vitro and in vivo applications.

504

505 **5. References**

- 506 [1] Bettinger C J, Langer R and Borenstein J T 2009 *Angew. Chem. Int. Ed. Engl.* **48** 5406-
507 15
- 508 [2] Gasiorowski J Z, Murphy C J and Nealey P F 2013 *Annu. Rev. Biomed. Eng.* **15** 155-76
- 509 [3] Kim H N, Jiao A, Hwang N S, Kim M S, Kang do H, Kim D H and Suh K Y 2013 *Adv.*
510 *Drug. Deliv. Rev.* **65** 536-58
- 511 [4] Joanne P, et al. 2016 *Biomaterials* **80** 157-168
- 512 [5] Kearns V R, Mc Murray R J and Dalby M J 2011 *Biomaterial surface topography to*
513 *control cellular response: technologies, cell behavior and biomedical applications*
514 *Surface modification of biomaterials Methods, analysis and applications (Oxford:*
515 *Woodhead Publishing Limited) pp 169-201*
- 516 [6] Goto M, Tsukahara T, Sato K and Kitamori T 2008 *Anal. Bioanal. Chem.* **390** 817-23
- 517 [7] Trantidou T, Terracciano C M, Kontziampasis D, Humphrey E J and Prodromakis T 2015
518 *Sci. Report* **5** 11067

- 519 [8] Singh A V, Patil R, Thombre D K and Gade W N 2013 *J. Biomed. Mater. Res. Part A* **101**
520 3019-3032
- 521 [9] Anselme K, Davidson P, Popa A M, Giazzon M, Liley M and Ploux L *Acta Biomater.*
522 2010 **6** 3824-46
- 523 [10] Idota N, Tsukahara T, Sato K, Okano T and Kitamori T 2009 *Biomaterials* **30** 2095-101
- 524 [11] Wood M A 2007 *J. R. Soc. Interface* **4** 1-17
- 525 [12] O'Connell C D, Higgins M J, Moulton S E and Wallace G G 2015 *J. Mater. Chem. C* **3**
526 6431-6444
- 527 [13] Ruiz S A and Chen C S *Soft Matter* 2007 **3** 168-177
- 528 [14] Dalby M J, Pasqui D and Affrossman S *IEEE Proc. Nanobiotechnol.* **151** 53-61
- 529 [15] Jayasinghe S N 2013 *Analyst* **138** 2215-23
- 530 [16] Spijker H T, Bos R, Busscher H J, van Kooten T G and van Oeveren W 2002
531 *Biomaterials* **23** 757-766
- 532 [17] Tsougeni K, Vourdas N, Tserepi A and Gogolides E 2009 *Langmuir* **25** 11748-11759
- 533 [18] Tsougeni K, Bourkoula A, Petrou P, Tserepi A, Kakabakos S E and Gogolides E 2014
534 *Microelectron. Eng.* **124** 47-52
- 535 [19] Gogolides E, Constantoudis V, Kokkoris G, Kontziampasis D, Tsougeni K, Boulousis G,
536 Vlachopoulou M and Tserepi A 2011 *J. Phys. D: Applied Physics* **44**, 174021.
- 537 [20] Gogolides E, Ellinas K and Tserepi A 2015 *Microelectron. Eng.* **132** 135-155
- 538 [21] Vourdas N, Kontziampasis D, Kokkoris G, Constantoudis V, Goodyear A, Tserepi A,
539 Cooke M and Gogolides E 2010 *Nanotechnology* **21** 085302.
- 540 [22] Kontziampasis D, Constantoudis V and Gogolides E 2012 *Plasma Proc. Polymer* **9** 866-
541 872.
- 542 [23] Tserepi A, Gogolides E, Bourkoula A, Kanioura A, Kokkoris G, Petrou P S and
543 Kakabakos S E *Plasma Chem. Plasma Proc.* 2016 **36** 107-120
- 544 [24] Loesberg W A, Riet J, van Delft F C M J M, Schön P, Figdor C G, Speller S, van Loon
545 J J W A, Walboomers X F and Jansen J A 2007 *Biomaterials* **28** 3944-51
- 546 [25] Dalby M J, Riehle M O, Johnstone H, Affrossman S and Curtis A S 2002 *Biomaterials*
547 **14** 2945-54
- 548 [26] Dalby M J, Riehle M O, Johnstone H J, Affrossman S and Curtis A S 2002 *Tissue Eng.*
549 **8** 1099-108
- 550 [27] Kunzler T P, Huwiler C, Drobek T, Vörös J and Spencer N D 2007 *Biomaterials* **28**
551 5000-6

- 552 [28] Li B and Logan B E 2004 Colloid Surf. B Biointerfaces **36** 81-90
- 553 [29] Webster T-J and Ejiogor J U 2004 Biomaterials **25** 4731-9
- 554 [30] de Oliveira P T, Zalzal S F, Beloti M M, Rosa A L and Nanci A 2007 J. Biomed. Mater.
555 Res. A **80** 554-64
- 556 [31] Fan Y W, Cui F Z, Hou S P, Xu Q Y, Chen L N and Lee I S 2002 J. Neurosci. Methods
557 **120** 17-23
- 558 [32] Gentile F, Tirinato L, Battista E, Causa F, Liberale C and Decuzzi P 2010 Biomaterials
559 **31** 7205-7212
- 560 [33] Davidson P M, Bigerelle M, Reiter G and Anselme K 2015 Biointerphases **10**
561 031004
- 562 [34] Kontziampasis D, Bourkoula A, Petrou P, Tserepi A, Kakabakos S and Gogolides E
563 2013 Proc. SPIE **8765** 87650B
- 564 [35] Decuzzi P and Ferrari M 2006 Biomaterials **27** 5307-5314
- 565 [36] Ivanova E P, et al. 2012 Small **8** 2489-2494
- 566 [37] Pogodin S, et al. 2013 Biophys. J. **104** 835-840
- 567 [38] Efremov Y M, Lomakina M E, Bagrov D V, Makhnovskiy P I, Alexandrova A Y,
568 Kirpichnikov M P and Shaitan K V 2014 Biochim. Biophys. Acta **1843** 1013-1019
- 569 [39] Constantoudis V, Patsis G P, Leunissen L H A and Gogolides E 2004 J. Vac. Sci.
570 Technol. B **22**, 1974 -1981
- 571 [40] Xue F, Liu J, Guo L, Zhang L, Li Q 2015 J. Theor. Biol. **385** 1-7
- 572 [41] Tsougeni K, Vourdas N, Tserepi A and Gogolides E, 2015 ACS Appl. Mater. Interfaces
573 **7** 14670–14681
- 574 [42] Huth F, Govyadinov A, Amarie S, Nuansing W, Keilmann F and Hillenbrand R 2012
575 Nano Lett. **12** 3973–3978
576
- 577 [43] Emmons E D, Kraus R G, Duvvuri S S, Thompson J S and Covington A M 2007 J.
578 Polym. Sci. Part B: Polym. Phys. **45** 358–367